Colloids and Surfaces A: Physicochemical and Engineering Aspects 613 (2021) 126086

Contents lists available at ScienceDirect

Colloids and Surfaces A: Physicochemical and Engineering Aspects

journal homepage: www.elsevier.com/locate/colsurfa

A versatile strategy to synthesize sugar ligand coated superparamagnetic iron oxide nanoparticles and investigation of their antibacterial activity

Giovanni Marco Saladino [a], Bejan Hamawandi [a], Mehmet Ali Demir [b], Idris Yazgan [b,*], Muhammet Sadaka Toprak [a,*]

[a] Department of Applied Physics, Biomedical and X-Ray Physics, KTH – Royal Institute of Technology, SE 10691, Stockholm, Sweden
[b] Department of Biology, Center of Biosensors and Materials, Kastamonu University, 37150, Kastamonu, Turkey

GRAPHICAL ABSTRACT

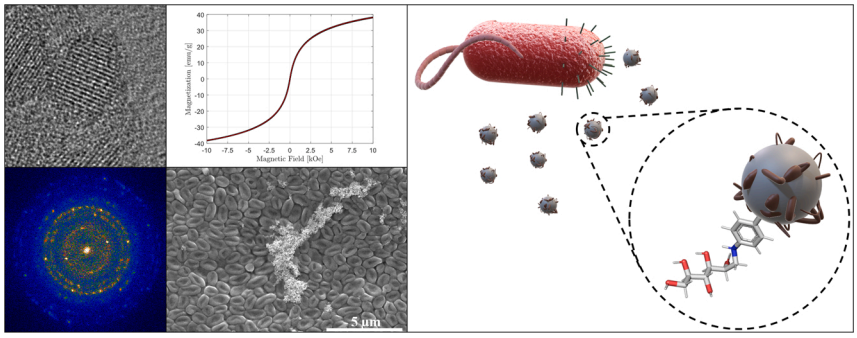

ARTICLE INFO

Keywords:
Sugar ligands
Iron oxide
Antibacterial properties
Bactericide nanoparticles
Superparamagnetic nanoparticles
Microwave-assisted synthesis

ABSTRACT

For the time being, a great attention has been given to the search of green and reusable materials with antibacterial properties. The present research focused on the design and synthesis of hybrid structures constituting superparamagnetic iron oxide nanoparticles (SPIONs) coated with sugar ligands (SL), synthesized using a green and efficient microwave (MW)-assisted hydrothermal synthesis. The sugar ligands were selectively engineered to obtain antibacterial characteristics towards multi-drug resistant bacterial strains, which are among the most problematic bacterial species in antibiotic development efforts. The superparamagnetic behavior was obtained by synthesizing core iron oxide nanoparticles with a diameter below twenty nm. The MW-assisted hydrothermal method yielded a uniform coating of SPIONs with several sugar ligands, granting strongly negative-charged surfaces, which have eventually contributed to their bactericidal activity. The research work allowed to get insights into the magnetic properties of the sugar ligand coated SPIONs, as well as on morphological and functional characteristics of the hybrid nanoparticles, by employing both spectroscopy and imaging techniques, such as FT-IR, Scanning/Transmission Electron Microscopy (S/TEM). Detailed characterizations of the nanoparticles' charge, using zeta potential analysis helped to identify the highly charged hybrids for antibacterial applications. Furthermore, studies on the bactericidal properties of selected SL-SPION hybrids highlighted a high selectivity towards both gram-negative and gram-positive bacteria along with improving bactericidal activity of streptomycin/penicillin mixture. Detailed studies done on *Pseudomonas aeruginosa* revealed that the SPIONs

* Corresponding authors.
E-mail addresses: iyazgan@kastamonu.edu.tr (I. Yazgan), toprak@kth.se (M.S. Toprak).

https://doi.org/10.1016/j.colsurfa.2020.126086
Received 25 October 2020; Received in revised form 11 December 2020; Accepted 16 December 2020
Available online 29 December 2020

selectively downregulated the virulence factor pyoverdine and altered bacterial morphology depending on the SL chemistry. The synthesized materials with antibacterial activity pave the way for an effective path towards the design and development of nanostructures and coatings against antibiotic-resistant bacterial species.

1. Introduction

In recent years, the interest towards the design of hybrid nanostructured materials with antibacterial properties have increased [1]. Nanomaterials with multi-functional capabilities, which can be tuned for specific tasks, are of growing interest [2]. Nanoparticles (NPs) have gained recognition as ideal synthetic building blocks for the development of a plethora of nanomaterials. In this context, green and facile synthesis of NPs with controlled size and morphology has been playing an important role [3]. Magnetic NPs have attracted significant attention due to their unusual properties, significantly differing from their bulk counterparts. Their high specific surface area, and tunable physicochemical properties through their size control make them attractive for many applications. Iron oxide NPs (in the form of magnetite, Fe_3O_4, or maghemite -Fe_2O_3) have found applications in several environment-friendly and biomedical areas, from food industry [4] to water remediation [5], sensors [6], cancer diagnosis [7] and therapy [8]. Superparamagnetic properties exhibited by iron oxide NPs with diameters lower than 20 nm have led to an extensive usage, because of the possibility of magnetizing the NPs when only biased by an external magnetic field, for magnetic separation [9] and hyperthermia studies [10].

Many synthesis routes for superparamagnetic iron oxide NPs (SPIONs) have been proposed in recent years but a few constitutes valid and efficient methods [11]. In particular, microwave (MW)-assisted hydrothermal methods have exhibited high scalability and NPs with highly reproducible quality and properties [12]. Green synthesis methods can grant a valid path for the development of NPs for biomedical applications [13,14]. The interest towards the surface functionalization of NPs has grown because of the possibility to use customized and specific molecules to enhance specificity for a wide range of applications [15]. Furthermore, the possibility to generate hybrids with SPIONs has been explored and reported [16]. Specifically, we recently reported on a novel one-step method for the synthesis of citrate-functionalized SPIONs, by employing a MW-assisted hydrothermal method, granting a bio-compatible and environment-friendly process [17]. Recently, research efforts have intensified on developing new strategies to fabricate hybrid materials with capping ligands made of carbohydrates [18–20], due to their potential applications in the design and development of nano-devices and nanosensors for bio-medical applications [21,22]. Carbohydrates possess many hydroxyl and carbonyl groups, which offer sugar coated NPs unique capabilities, providing them with attractive attributes for building smart nanomaterials.

Several mechanisms of actions of nanomaterials have been proposed to explain their bactericidal properties and selectivity but their behavior is still debated [23]. *Staphylococcus aureus (gram +)* [24], *Listeria monocytogenes* (gram +) [25] and *Klebsiella pneumoniae* (gram -) [26] are among detrimental bacterial species that can cause resistance towards a variety of antibiotics. NPs decorated with carbohydrates possessing advanced multivalence as potent drug and drug carrier have got great attention to overcome resistance developed by infectious bacterial strains [24]. Similarly, NPs are shown to be powerful additives as coating ingredient for fabric materials (e.g. surgical face masks) in order to eliminate infectious bacterial species [27]. The current work has, therefore, focused on the design and development of functionalized SPIONs with custom-made sugar ligands, which promote antibacterial activity, aiming at obtaining an efficient and reusable tool with bactericidal properties, where superparamagnetic NPs represent an optimal means for high dispersity and separation.

2. Materials and methods

2.1. Materials

Ferric chloride hexahydrate ($FeCl_3 \cdot 6H_2O$, 97 %), ferrous sulphate heptahydrate ($FeSO_4 \cdot 7H_2O$, 99 %), sodium hydroxide (NaOH, 98 %), D-mannose ($C_6H_{12}O_6$; ≥ 99 %), D-Sucrose ($C_{12}H_{22}O_{11}$; ≥ 99.5 %), D-Lactose monohydrate ($C_{12}H_{22}O_{11} \cdot H_2O$; ≥ 99.5 %), p-aminobenzoic acid ($H_2NC_6H_4CO_2H$; ≥ 99 %), 3-aminophenol ($H_2NC_6H_4OH$; ≥ 98 %), 4-aminophenyl sulfone, Borane dimethylamine complex (% 97) and p-phenylenediamine (≥ 99 %) were all purchased from Sigma Aldrich (Stockholm, Sweden).

2.2. Sugar ligands synthesis

Sugar ligands (SL) were synthesized using a two-step reductive amination reaction in 50:50 acetic acid:water solvent system [28,29]. Briefly, molar ratio of amino groups in the organic substituents to the sugar moieties were kept as 1.2 in order to fully deplete sugar content that allowed precipitation of final product (amine or imine form of sugar ligands) while residual organic groups were washed away by acetone and ethanol cleaning. In case of amine synthesis, borane dimethylamine complex (ratio was 1.2 to sugar residue) was used to convert imine intermediate into amine. In case further purification needed, hydrophilic liquid interaction chromatography was used [29].

2.3. Iron oxide nanoparticle synthesis

0.1 M and 0.05 M stock solutions were, respectively, prepared for ferric chloride and ferrous sulphate, in deionized (DI) water. Furthermore, SLs were dissolved in DI water to obtain a concentration of 0.02 M. Finally, a 1 M sodium hydroxide stock solution was prepared. A MW-assisted hydrothermal method was used to synthesize spherical coated iron oxide particles, as described earlier [17]. Equivalent volumes of ferric chloride and ferrous sulphate (8 mL) were mixed under magnetic stirring. Subsequently, 3.4 mL of NaOH was rapidly introduced and 8 mL from the SL stock solution was added. The mixture was then processed under MW irradiation using flexi-WAVE (Milestone SRL, Milan, Italy) MW reactor at 2.45 GHz. The treatment duration was set to 25 min at 150 °C under continuous magnetic stirring, with a 5-min linear ramp (Figure S1). In a typical run, five different SL-SPIONs were synthesized in a single run using a multi-reactor carousel system in the MW reactor. For the subsequent characterizations, the sample was washed by centrifuging and re-dispersing three times with DI water, in order to remove the residual chemicals.

2.4. Antibacterial tests

10^4 cfu/mL inoculum from each of freshly prepared bacterial strains (i.e. *Enterococcus faecium* (*E.faecium,* gram +), *Enterobacter aerogenes* (*E. aerogenes,* gram -), *Escherichia coli* (*E.coli,* gram -), *Bacillus subtilis* (*B. subtilis,* gram +) and *Pseudomonas aeruginosa* (*P.aeruginosa,* gram +)) were placed in 2 mL of Nutrient Broth. Except for *E.coli*, all the strains are multi-drug drug-resistant (e.g. *E.aecium* has resistant to vancomycin, erythromycin and tetracyclines, and *P.aeruginosa* has resistance to β-lactams and quinolones). 75 μg/mL (if not specified otherwise) from the selected SPIONs were placed in the dedicated test tubes, where DI water was used as the control, which underwent 24 h incubation in 37 °C incubator (Illustrated in Supplementary Figure S7). Followed by incubation, 20 μL from each sample tube were placed on freshly prepared

agar for further incubation to visualize colonies, which underwent up to 48 h incubation at 37 °C. The grown colonies were dissected and placed in 2 mL of DI water followed by vortexing, for preparing a homogenous solution. The absorbance of obtained solutions was measured at 595 nm, which were used to calculate % decrease in growth. In all cases, if not mentioned otherwise, 10^4 cfu/mL bacteria were used for the antibacterial tests. In order to search synergistic effect of the SPIONs combined with classical antibiotics, penicillin/streptomycin mixture (Lonza, Cat number 09-757 F) was introduced into the medium at two different concentrations (i.e. 10 μL/2 mL and 20 μL/2 mL). In the case of *P.aeruginosa* growth, in order to enhance bluish green fluorescent molecule synthesis, fresh inoculums were prepared on agar, while for film formation and growth on SPION coated fabrics the fresh inoculum was prepared in broth (this is a long-term practice in our lab).

Determination of P. aeruginosa biofilm formation in plastic tubes: 10^4 cfu/mL of *P. aeruginosa* was grown in 2 mL of Nutrient Broth, in which 75 μg/mL of SPIONs was introduced. Followed by 24 h incubation, the medium was decanted and the tubes were rinsed with PBS buffer (pH 7.2) for three times. 2 mL of crystal violet (0.2 % in DI water) was then introduced to the tubes and reacted for 30 min. Unbound crystal violet solution was removed, and the tubes were rinsed three times with PBS buffer (pH 7.2). 2 mL of 95 % ethanol was added to the tubes and incubated for 20 min for a complete dissolution of the bound crystal violet, whose absorbance was measured at 530 nm.

Antibacterial activity of the coated fabrics on *P. aeruginosa* were tested using AATCC 100-1999 as described elsewhere [27]. %100 cotton fabric with 1 cm^2 area and 0.5 mm thickness was rinsed with 70 % ethanol for 5 min, followed by sterilization under UV for 15 min. A 25 μL aliquot of SPION solution was dropped on the sterile fabric and dried under sterile conditions, followed by 15 min UV exposure. In addition to this, *P.aeruginosa* growth on the coated fabric was performed as well ($1-2$ cm^2 cotton fabrics were used, and amount of SPIONs were adjusted in relation to the surface area). In all cases, free SPIONs were removed using sterile PBS buffer (pH 7.2). Scanning Electron Microscopy was used to visualize bacterial growth on the surfaces.

2.5. Characterization techniques

Surface potential (ζ-potential) values of NPs were measured with Zetasizer Nano ZS90 at an incident angle of 90° (Malvern Instruments, Malvern, Worcestershire, United Kingdom). The samples were prepared by diluting in distilled water, and measurements were performed at room temperature in triplicates. Mass spectrometry (MS) (Shimadzu LCMS-8030 Plus, Kyoto, Japan) was used for the characterization of the SLs. Thermal gravimetric analysis (TGA) was executed by employing TGA 55 (TA Instruments, Stockholm, Sweden) system in order to quantify the organic content in each sample. The samples were dried and subsequently heated from 25 °C to 900 °C with a heating rate of 20 °C/min under synthetic air. Fourier-transform infrared spectroscopy (FT-IR, Thermo Scientific Nicolet iS20, Stockholm, Sweden) was performed to study the surface exposed groups of pure sugar ligands as well as the NPs with sugar-capping. The FT-IR spectra were obtained in the transmission mode using the KBr pellet mode (KBr Mini-Pellet Press, Specac, SigmaAldrich, Stockholm, Sweden) in the spectral range of 4000 to 450 cm^{-1}. Dried samples were analyzed with Vibrating-Sample Magnetometry (VSM, Lake Shore 7300-series, USA). The magnetic field ranged from -10 to +10 kOe (double scan) in order to obtain the magnetization curves of SL capped NPs. Powder X-ray Diffraction (PXRD) was used to identify the crystalline phases present on a PANalytical X'Pert PRO system, equipped with a Copper anode (Cu–K radiation) using a step size of 0.24° in continuous mode and a scan speed of 0.04°/s. Scanning Electron Microscopy (SEM, FEI Nova 200, Hillsboro, OR, USA) was employed to obtain an overview of the dried samples, by imaging with an acceleration voltage of 10 keV. A graphite-coated aluminum holder was used, where 20 μL samples were dropped and air dried. Transmission Electron Microscopy (TEM, JEM-2100 F, 200 kV, JEOL, Tokyo, Japan) was used to study NPs morphology, size and crystallinity, by drop casting and drying 20 μL of sample on a copper grid. Inductively coupled plasma–optical emission spectroscopy (ICP-OES, SpectroBlue, Spectro) was used for the determination of elemental Fe concentration in the colloidal suspensions prior to antibacterial tests.

3. Results and discussion

3.1. Nanoparticle characterization

For the synthesis of NPs, a collection of sugar ligands (SLs) was prepared, in order to obtain differently functionalized SPIONs and, thus, different antibacterial properties. The catalogue of SLs is presented in the Supplementary Materials, showing the molecular structure of ten different ligands used as functionalizing -or surface capping, agents (Figure S2). Molecular weight of all the SLs were determined by MS, and the obtained mass spectra are presented in Figure S3. Calculated molecular weights are ~288 Da (MpAB), ~451 Da (CBpAB), ~451 Da (SZpAB), ~524 Da (LODA-N), ~433 Da (L3AP), ~431 Da (L3APimin), ~477 Da (L5AS), ~315 Da (G5AS), ~432 Da (GPDA) and ~896 Da (SZPSA), in agreement with the presented molecular formula.

The washed stock solutions resulted in ten black-colored samples. These were first characterized by studying their surface charge and surface chemistry using zeta (ζ) potential analysis and FT-IR spectroscopy. The ζ-potentials of the bare SPION and SL coated SPIONs (SL-SPIONs), in distilled water (pH measured as 6.5), are summarized in Table 1. Bare SPION synthesized in the absence of any sugar ligands resulted in a zeta potential of −43 mV. All the SL functionalized samples showed lower negative surface charges, thus indicating the successful functionalization of SPIONs. The FT-IR spectra of the samples were compared with the corresponding SL powders, which confirmed the presence of traces of SL in the washed stock solutions (Figure S4). From the collection of SL-SPIONs, the four highly charged samples (one for each sugar group mannose, sucrose, lactose and galactose) were chosen for further analyses. The strong negative charge, indeed, induced a greater colloidal stabilization of the NPs in the dispersion, hence avoiding the formation of agglomerates and sedimentation.

The molecular structure of SLs corresponding to the four selected samples are presented in Fig. 1; all the four ligands are characterized by the presence of hydroxyl groups, responsible of the partial neutralization of the negative charge possessed by the bare SPIONs.

In Fig. 2, the FT-IR spectra for the selected SL coated NPs are displayed, compared to the corresponding SL powders. The wide band in the range 3000-3700 cm^{-1} is present in all the four SL and related SL-SPIONs; this range corresponds to the OH stretching of the ligands and to the adsorbed water molecules on the surface of the NPs. Below 700 cm^{-1}, the Fe-O stretching in the crystalline structure of SPIONs is shown [30]. MpAB-SPIONs, showed sharp peaks in the range 1480-1750

Table 1
ζ-potentials for the bare SPIONs and SL-SPIONs in water (pH = 6.5), summarizing the employed sugar ligands (SL). SL functionalized SPIONs with highest charged surfaces are shaded grey. For complete names and molecular structure of SLs see Supplementary Information Table S1 and Figure S2.

SL-SION Samples	ζ-Potential [mV]
Bare SPIONs	−43.0
MpAB-SPIONs	−18.2
CBpAB-SPIONs	−6.0
SZ-pAB-SPIONs	−5.4
L-ODA-N-SPIONs	−7.0
L3AP-SPIONs	−2.2
L3APimin-SPIONs	−27.0
L-5AS-SPIONs	−3.6
G-5AS-SPIONs	−8.3
G-PDA-SPIONs	−8.7
SZ-PSA-SPIONs	−24.0

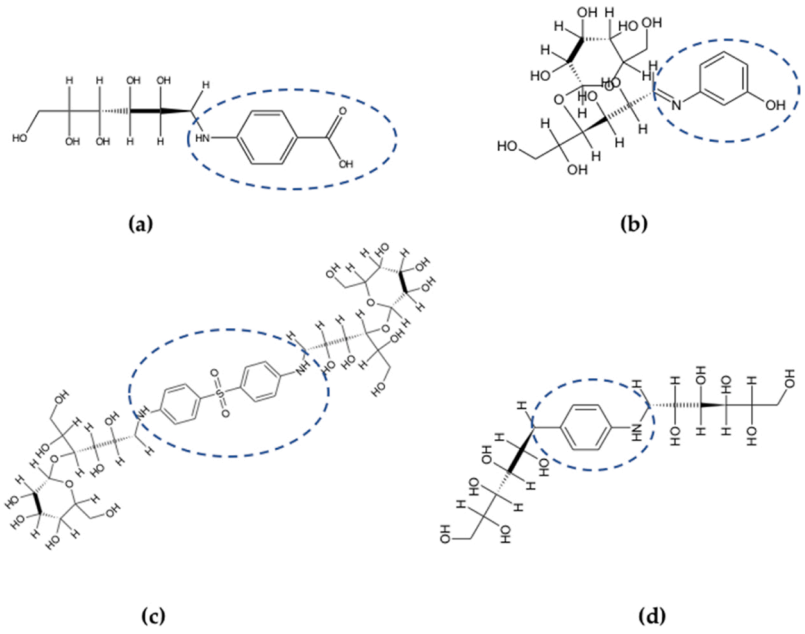

Fig. 1. Molecular structures of the SLs yielding highly charged surfaces on functionalized SPIONs, MpAB (a), L3APimin (b), SZ-PSA (c) and G-PDA (d). Functionality added to the sugar is encircled for clarity. For complete names and molecular structure of SLs see Supplementary Information, Table S1 and Figure S2.

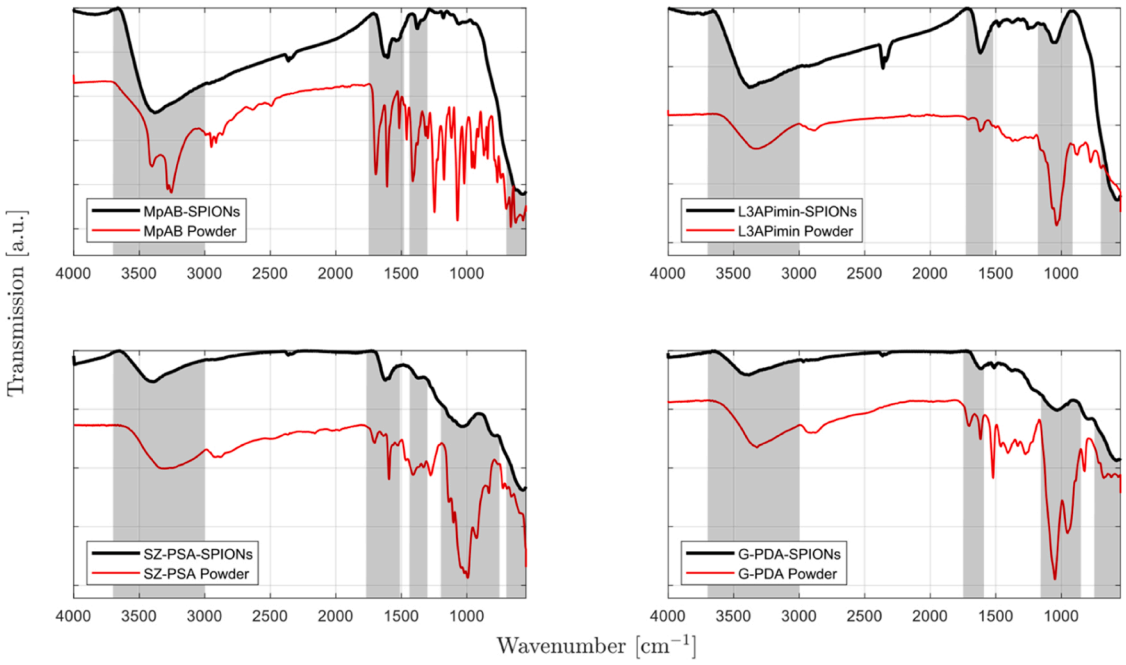

Fig. 2. FTIR spectra for the selected SL-SPIONs and corresponding SL powders, MpAB, L3APimin, SZ-PSA and G-PDA. For complete names and molecular structure of SLs see Supplementary Information, Table S1 and Figure S2.

cm^{-1}, for CO stretching and CC═══ skeletal vibrations of the benzyl group, and 1300-1440 cm^{-1} for CH and OH—— bending modes. An important observation is the decrease in the number of bands due to carbonyl (C═O) and carboxyl CO— absorptions, which reduce to a single band in the MpAB-SPIONs. This indicated a strong interaction between the carboxyl group on the MpAB SL with the surface of SPION. L3APimin-SPION and corresponding SL exhibit the C = N- stretching at 1520-1730 cm^{-1} and a strong broad peak at ~ 1050 cm^{-1} for CO— stretching vibration of (primary or secondary) alcohols [31], also clearly identifiable in SZ-PSA and G-PDA, and related coated NPs. Regarding SZ-PSA-SPION, the characteristic peak for S═O stretching mode is highlighted at ~ 1400 cm^{-1}. Finally, at 1600 cm^{-1}, it is possible to observe the N—H bending mode of secondary amine both for SZ-PSA-SPIONs and G-PDA-SPIONs, mirroring the related SL's structure. This detailed comparative analysis has thus confirmed the successful binding of the SLs on the SPIONs' surface, without substantially altering their chemical structures. The FT-IR spectra for the other SL-SPIONs are shown in the Supplementary Information – Figure S4, highlighting the successful functionalization for all the SPION samples.

Aiming at identifying the composition by weight, or weight ratio between the SL coating and the magnetic iron oxide core of SPIONs, a thermogravimetric analysis (TGA) was performed on the selected SL-

SPIONs; the resultant thermograms are presented in Fig. 3 where the weight change (in percentage) is shown as a function of the temperature. The thermograms were split into several regions at the inflection points to highlight the numerous steps of organic decomposition. The region I is analogous in all the four samples and identifies water desorption from the NPs surfaces. The water content in the dried NPs constitutes about 4–10 % of the total weight, whilst the amount of SLs has been found to be strongly related to their complexity; the ligand coated MpAB-SPIONs surface is the simplest among the chosen ones and led to the lowest ligand-core ratio, equal to 7%, and a straightforward decomposition trend, with only one intermediate region before reaching the steady state.

With an intermediate complexity, L3APimin yielded a ratio of 20 % to the SL coated NPs and a subdivision into a total of four regions, where the sugar decomposition is split into two steps (region II and III). Furthermore, SZ-PSA- and G-PDA-SPIONs exhibit a sugar-core ratio of 25 % and 32 %, respectively, still confirming the fact that high molecular weights lead to high sugar-core ratios. In particular, the ligand decomposition occurs in three steps – highlighted as region II, III and IV in the plots – in the two latest samples, reaching a steady state at 820 °C and 850 °C, respectively. The above-discussed analysis permitted to estimate the relative amount of magnetic core in functionalized SPIONs, of great relevance when attaining magnetic characterization and estimating the saturation magnetization (per unit weight), and the magnetic diameter. The analysis showed that an increased complexity of the SL considerably affects the total coating ligand content of functionalized SPIONs.

The selected samples were characterized for their magnetic properties by employing a Vibrating-sample magnetometer. All samples exhibited superparamagnetic behavior, as can be observed in Fig. 4.

The magnetic characteristics were extrapolated via the software SPfit [17,32], allowing to fit the magnetization curve to the ideal behavior, given by the following relation:

$$M = M_S \int_0^\infty L(y)f(y)dy$$

where M is the magnetization, M_S is the saturation magnetization, $f(y)$ is the size distribution of NPs with reduced diameter y and $L(y)$ is the Langevin function [33]. Saturation magnetization, magnetic coercivity and inorganic content of the SL-SPIONs for the selected four samples were reported in Table 2.

The weight percent of the magnetic cores was considered through the analysis of the TGA results. Employing the mass of the cores and their magnetic behavior, L3APimin-SPION exhibited the highest saturation magnetization of 72.2 emu/g, and magnetic core diameter of 5.7 nm. All the samples have their magnetic core diameter in the range 4−6 nm,

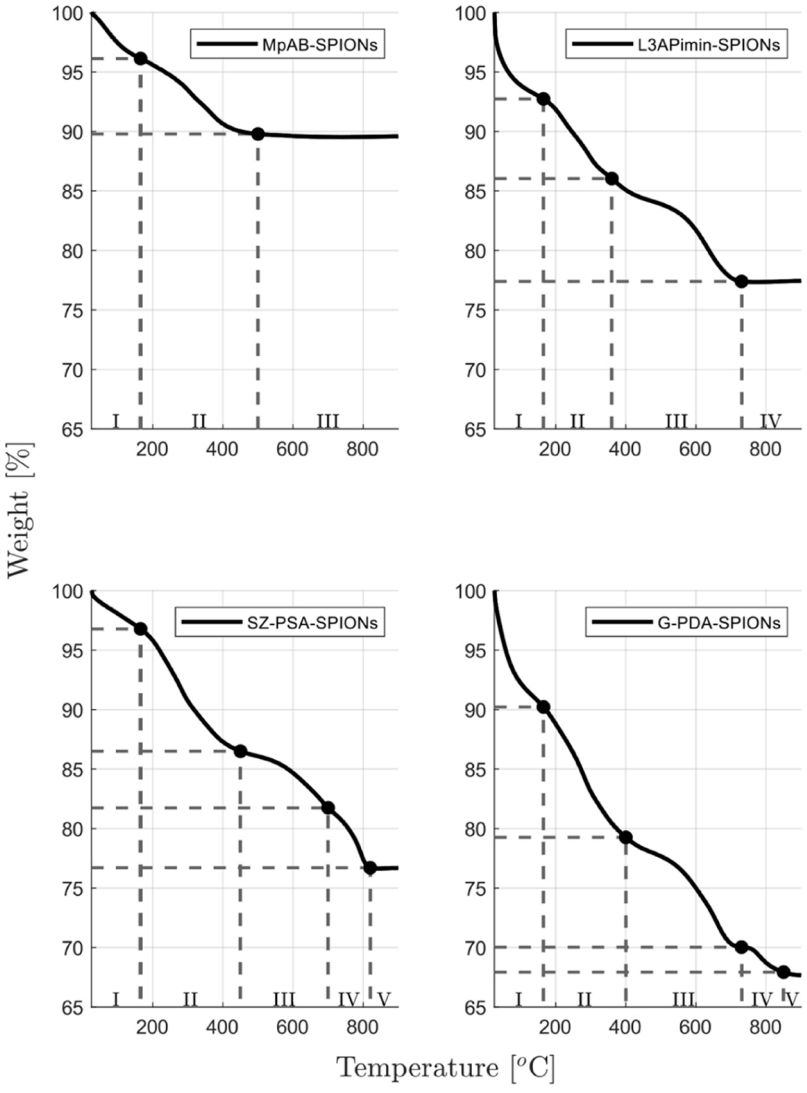

Fig. 3. TGA thermograms for the four selected SL-SPIONs functionalized with MpAB, L3APimin, SZ-PSA and G-PDA SLs. For complete names and molecular structure of SLs see Supplementary Information, Table S1 and Figure S2.

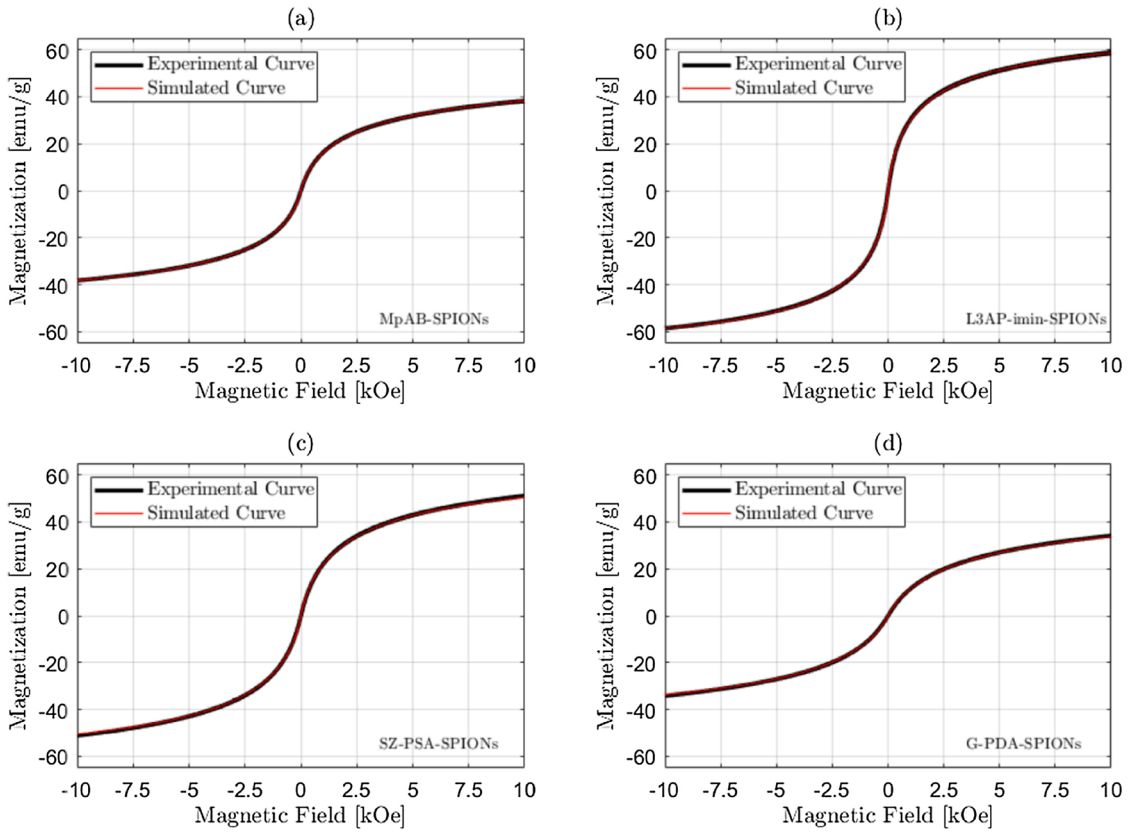

Fig. 4. Experimental and simulated magnetization curves for the MpAB-SPION (a), L3AP-imin-SPION (b), SZ-PSA-SPION (c), and G-PDA-SPION (d). For complete names and molecular structure of SLs see Supplementary Information, Table S1 and Figure S2.

Table 2
Magnetic properties of the four selected SPIONs functionalized with MpAB, L3APimin, SZ-PSA and G-PDA SLs. For complete names and molecular structure of SLs see Supplementary Information, Table S1 and Figure S2.

Sample	Saturation Magnetization [emu/g]	Magnetic Coercivity [Oe]	Inorganic Content [%]
MpAB-SPION	52.4 ± 0.5	1.1 ± 0.1	90
L3APimin-SPION	72.2 ± 1.0	1.3 ± 0.1	77
SZ-PSA-SPION	66.0 ± 5.1	1.3 ± 0.1	77
G-PDA-SPION	49.2 ± 4.9	1.2 ± 0.1	68

which definitely falls in the superparamagnetic size range for iron oxide at room temperature, confirmed by a low magnetic coercivity of the order of 1 Oe. The NPs synthesis is not significantly influenced by the SLs, when equal concentrations of SLs were used for a given amount of iron precursor. However, this is a ratio that can be tuned to result in differently sized SPIONs, without any additional chemicals used in the process. The presence of SLs does not affect the magnetic behavior of the cores, as expected.

SEM micrographs on these samples are presented in Supplementary Information, Figure S5, where small size of SPION are clearly distinguishable, with a layer constituted by condensed sugar ligands, forming a network of SPIONs. TEM analysis was performed for a closer investigation on these samples and few micrographs along with the FFT patterns are presented in Fig. 5. It is important to note that NPs are highly crystalline and measured lattice spaces are marked with their respective Miller indices in Fig. 5e, indexed to the cubic structure of Fe_3O_4 (International Centre for Diffraction Data ICDD PDF no. 01-088-0315). SPIONs are observed to be single crystalline as visualized from the HR TEM micrographs presented in Fig. 5e-h. PXRD performed on these samples are presented in Supplementary Information, Figure S6. In Table 3, a summary of the estimations of NPs' size obtained from different analysis techniques is presented. Particle size from TEM is slightly larger than, or the same as, the magnetic domain size estimated from VSM measurements. This shows a very reasonable agreement on the particle size obtained from two different techniques, where TEM size is generally slightly larger due to the presence of highly disordered, magnetically dead surface layer.

3.2. Antibacterial tests

Antibacterial activity of the SPIONs was tested for 48 h incubation period (Fig. 6) and the results are summarized in Table 4. SPIONs' toxicity on the tested bacterial strains are sensitive to the SPIONs' surface chemistry. Bare SPIONs and L3APimin-SPION showed their highest toxicities – over 50 % – on *E. coli* and *P. aeruginosa* whilst the strongest effect of MpAB-SPION was found for *E. coli*, *E. aerogenes* and *P. aeruginosa*. SZ-PSA-SPION strongly downregulated the growth of *E. aerogenes* and *P. aeruginosa* while G-PDA-SPION only decreased the growth of *E. coli* at over 50 %. Interestingly, G-PDA-SPION did not show any toxicity on *B. subtilis*, where *E. faecium* showed the highest resistance towards all the tested SPIONs. The findings cannot be simply explained by the surface charge of SPIONs since the same SPIONs did not reveal their toxicity based on gram (-) and gram (+) characters of the tested bacteria. Bacterial cells pose negatively charged cell surfaces, which affect their interaction with the surfaces and the surrounding. However, there is no linear interaction for the attraction between positively charged entities and negatively charged cell surfaces [34]. Another important phenomenon is negatively charged NPs are not cytotoxic, rather they alter bacterial metabolisms [35].

The SL toxicity at 1 mg/mL towards the tested bacterial species also showed that chemistry of the SL played an important role on revealing

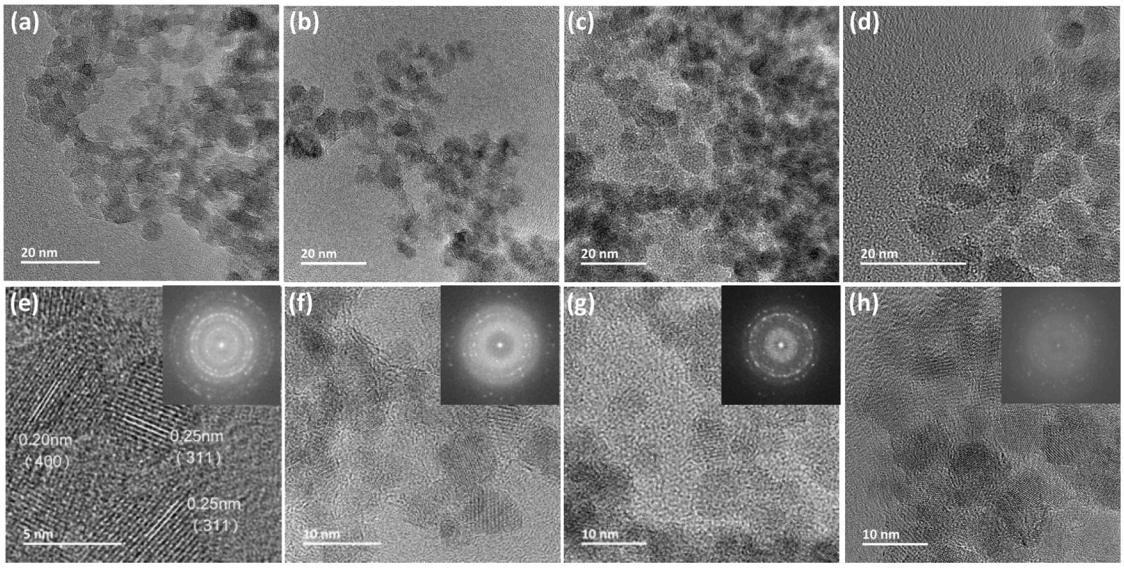

Fig. 5. TEM micrographs for MpAB-SPION (a,e), L3AP-imin-SPION (b,f), SZ-PSA-SPION (c,g), and G-PDA-SPION (d,h). Insets in micrographs (e-h) represent the FFT for the given samples. (For complete names and molecular structure of SLs see Supplementary Information, Table S1 and Figure S2.).

Table 3
Estimated particle size (TEM size) and magnetic domain size (magnetic diameter), accompanied with standard deviation, of the four selected SL-SPIONs, by using different techniques. For complete names and molecular structure of SLs see Supplementary Information, Table S1 and Figure S2.

Sample	Magnetic Diameter [nm]	TEM Size [nm]
MpAB-SPION	4.7 ± 0.7	4.7 ± 0.9
L3APimin-SPION	5.7 ± 0.7	5.7 ± 1.3
SZ-PSA-SPION	5.0 ± 0.6	5.0 ± 0.7
G-PDA-SPION	4.2 ± 0.5	4.4 ± 1.0

the antibacterial effect, both on gram (+) and gram (-) bacteria, where L3APimin gave highest antibacterial activity with ~40–70 % decrease in bacterial growth. MpAB only gave anti-bacterial activity against *E.coli* with ~40 reduction in growth, which has mannose binding *FimH* lectin [36]. In contrast to this, G-PDA and SZ-PSA did not reveal any significant toxicity for the tested bacterial strains. Therefore, the main reason underlying SL-based effect of antibacterial activity of the SPIONs can be related to carbohydrate-lectin interactions. Even though different bacterial species can have the same, or similar lectins, differences in their carbohydrate recognition domain (CRD) can bring substantial effects to their selectivity and sensitivity towards simple carbohydrates and modified carbohydrates [37,38]. However, it is not straightforward to come up with a conclusion, since there is no reported crystal structure of lectins along with CRDs for the studied bacterial species (except *E.coli*).

E. faecium, *E. aerogenes*, *E. coli* and *B. subtilis* were treated with the SPIONs at 75 μg/mL combined with 10 μL of streptomycin/penicillin (Supplementary Figure S8). Interestingly, SZ-PSA SPIONs

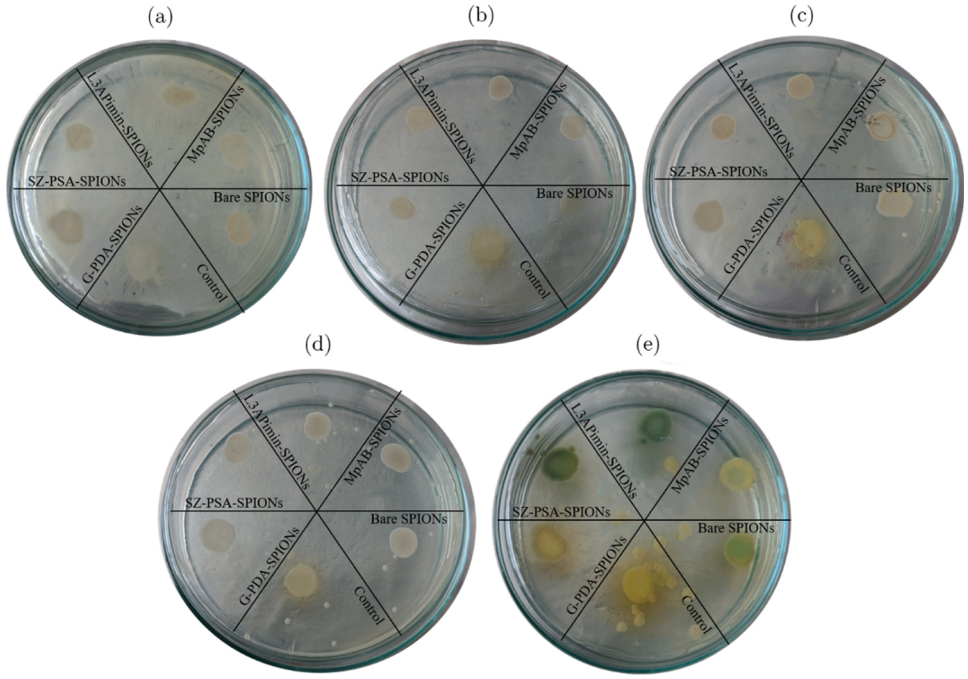

Fig. 6. Antibacterial activity of the SPIONs tested for 48 h incubation period; (a) *B. subtilis*, (b) *E. coli*, (c) *E. aerogenes*, (d) *E. faecium,* (e) *P. aeruginosa*.

Table 4
Antibacterial activity of the SPIONs tested for 48 h incubation period as percentage decrease in bacterial growth; Data in columns for: (a) *B. subtilis*, (b) *E. coli*, (c) *E. aerogenes*, (d) *E. faecium*, (e) *P. aeruginosa*.

Sample	Decrease in Growth [%]				
	a	b	c	d	e
Bare SPION	17	72	15	21	72
MpAB-SPION	35	53	54	18	63
L3APimin-SPION	42	56	46	19	72
SZ-PSA-SPION	36	41	53	27	58
G-PDA-SPION	0	78	48	12	42

antagonistically affected streptomycin/penicillin activity against *E.coli* treatment, where over 70 % of the growth sustained. In the case of *B. subtilis*, only bare SPION/streptomycin/penicillin and G-PDA SPION/streptomycin/penicillin fully eliminated bacterial growth, while the rest of the combinations and streptomycin/penicillin alone only eliminated about 95–99 %. None of the SPIONs revealed any antagonistic effect to streptomycin/penicillin for *E. faecium* and *E. aerogenes* treatment. Biofilm formation of these four bacterial strains were tested against the combinations, and dramatic findings were obtained (Supplementary Figure S8). Particularly, SZ-PSA SPIONs gave very strong antagonistic effect for streptomycin/penicillin treatment by increasing biofilm formation of *E.coli* ~ 1.9 times (alone SZ-PSA SPION only increased 1%), where streptomycin/penicillin alone treatment decreased the biofilm formation ~ 40 %. Similarly, G-PDA SPIONs antagonistically decreased antibiofilm activity of streptomycin/penicillin towards *E.aerogenes*, Except SZ-PSA SPION, rest of the SPIONs synergistically imrproved biofilm activity of streptomycin/penicillin by ~40−50% for *E.coli*. For the rest of the bacteria, only minor changes were observed. When the SPIONs were used alone to enlighten their effect on the biofilm formation, SZ-PSA SPION increased biofilm formation for all the strains in the range of 1–183 % range, where L3APimin-SPION triggered increases (except *B.subtilis* with 80 % decrease) were in the range 114–229 %. G-PDA SPION also increased biofilm formation (except *B.subtilis* by 25 % decrease) by 119–379 %, for which strains bare SPIONs only increased *E.aerogenes* biofilm formation by 19 % with reduction by 28–88 % for the rest of the strains (Supplementary Figure S12).

Antibacterial activity of the coated fabrics on *P.aeruginosa* were tested using a method described elsewhere [27]. The results revealed that the growth was suppressed by bare SPION, MpAB-SPION, L3APimin SPION, SZ-PSA-SPION and G-PDA-SPION by 61 %, 67 %, 75 %, 61 % and 45 %, respectively. These findings show that free SPION and corresponding coated fabric gave similar antibacterial activity against *P. aeruginosa*. *P.aeruginosa* growth was further tested on the selected SPIONs coated cotton fabric and biofilm formation, because it was the most sensitive strain for the SPIONs. Furthermore, it is producing green-colored pyoverdine, which is visible to bare eyes (or easily visualized with 365 nm hand-held flashlight), easing the detection of the variations.

Biofilm count of SPIONs introduced with 10^6 cfu/mL *P.aeruginosa* gave interesting results as bare SPION (80 μg/mL) decreased biofilm count by 28 % while MpAB- (75 μg/mL), L3Apimin- (75 μg/mL), SZ-PSA- (75 μg/mL) and G-PDA-SPIONs (100 μg/mL) increased biofilm formation by 54 %, 38 %, 57 % and 75 %, respectively. These results can be ascribed to the property of iron oxide NPs, posing stress on microorganisms, by which induction of biofilm formation is increased by *P. aeruginosa* [39–41].

Bare SPION decreased *P. aeruginosa* growth by 72 % and altered their morphology (lower aspect ratio, or length to width ratio), as can be seen from Fig. 7, leading to a decrease in biofilm amount. Decrease in the aspect ratio of bacteria was reported earlier for other NPs, such as ZnO [37], which was attributed to NP uptake and their effect on the cellular membrane. Bare SPION did inhibit pyoverdine production for 24 h incubation period while *P. aeruginosa* gave distinct green color of pyoverdine within 24 h incubation period (Fig. 8a), in which the excess pyoverdine disappeared from 24 to 48 h incubation (Fig. 6e). In the case of utilization of 75 μg/mL bare SPIONs for 10^4 cfu/25 μL *P.aeruginosa* inoculum resulted in 10 % decrease in the growth with still bare-eye visible bluish green color formation and 17 % increase in biofilm formation. Combination of bare SPION with 20 μL and 10 μL of streptomycin/penicillin resulted in total elimination of bacterial growth and biofilm formation, at which concentration streptomycin/penicillin gave the same result (Supplementary Figure S9). It is noteworthy to mention that 72 h incubation resulted in growth of *P. aeruginosa* with bare-eye visible green fluorescent molecules for bare SPION/10 μL of streptomycin/penicillin treatment, at which incubation period 20 μL of streptomycin/penicillin treatment did not prevent the growth (Supplementary Figure S10). In contrast to this, 10 μL of

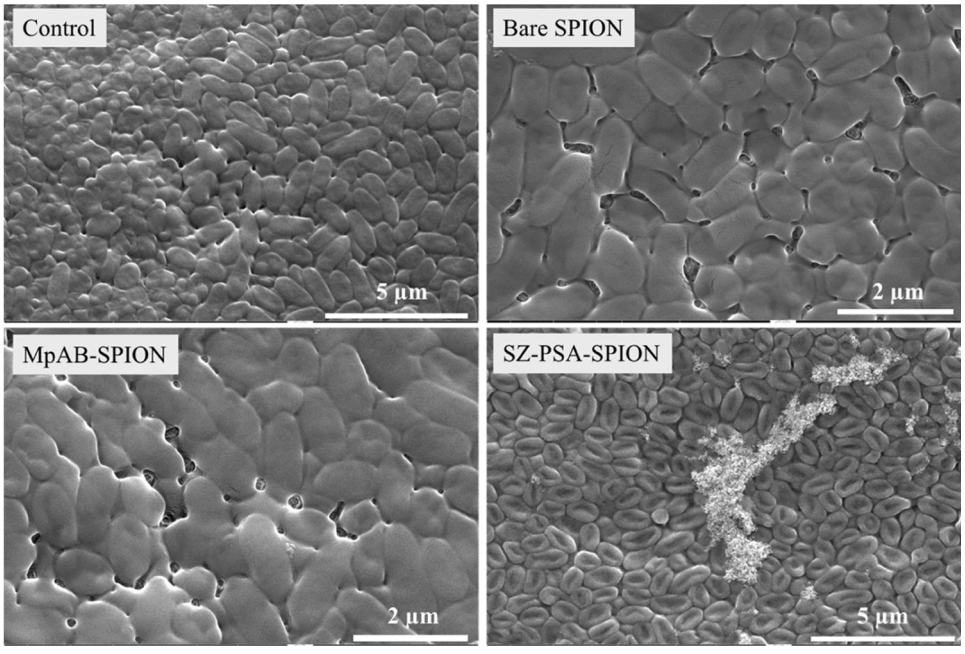

Fig. 7. SEM micrographs of the bare and selected SL-SPIONs coated fabrics, along with the untreated control sample.

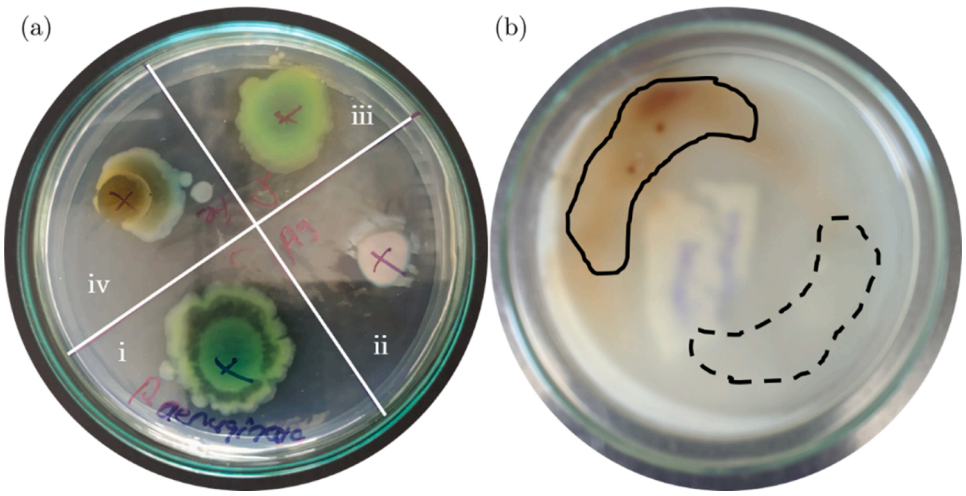

Fig. 8. (a) *P. Aeruginosa* (i) response towards silver (ii), copper (iii) and iron ions (iv) on solid agar for 24 h incubation period, and (b) for MpAB-SPIONs treatment (solid area) on soft agar for 24 h incubation period. Soft agar was the same as solid agar, which was poured when the Nutrient Agar was hot (~ 70 °C).

streptomycin/penicillin did only decrease the growth of *P. aeruginosa* by 40 %, and 93 % biofilm formation in the case of 10^6 cfu/25 μL, where combination with bare SPIONs only decreased the biofilm formation by 73 % (Supplementary Figure S10). Under these conditions, bare SPIONs gave antagonistic effect.

MpAB-SPION did not alter the morphology (Fig. 7, MpAB-SPION) of the bacteria, while it decreased the growth over 60 %. Produced green-colored pyoverdine by *P. aeruginosa* [38], which is an important iron-scavenging siderophore required for pathogenesis of *P. aeruginosa* [42]. As seen from Fig. 6, MpAB downregulated production of pyoverdine throughout 48 h incubation, which is related to the stress exposed by MpAB-SPIONs. Therefore, it is possible that *P. aeruginosa* altered its metabolism for larger biofilm development (54 % increase) in the case of 10^6 cfu/25 μL inoculum utilization (Supplementary Figure S11), where combination with 10 μL of streptomycin/penicillin resulted in 95 % decrease in biofilm formation in the case 10^6 cfu/25 μL inoculum utilization. Combination of MpAB-SPION (75 μg/mL) 20 μL and10 μL mixture of streptomycin/penicillin resulted in 100 % decrease of biofilm formation and growth, whereas MpAB-SPION did not cause any decrease in biofilm formation and led to only 10 % decrease in the growth (Supplementary Figure S8). However, increasing incubation time to 72 h resulted in *P. aeruginosa* growth for MpAB-SPION/10 μL penicillin/streptomycin mixture.

SZ-PSA did alter the morphology (Fig. 7, SL7) of *P. aeruginosa*; SZ-PSA-SPIONs treatment decreased the strength of the cell membrane of *P. aeruginosa*, which resulted in collapse of the cells upon drying process. Damaging bacterial membranes by NPs (e.g. CuO, ZnO, AgNPs) is a commonly observed phenomenon [43–45]. This membrane damage can be linked to alteration in bacterial metabolism [35]. However, when the surface of the fabric was thoroughly rinsed with PBS buffer (pH 7.2) to remove the bacteria on the surface, the bacteria on top of the cotton did not show any alteration (data now shown). This means that the stress effect of SZ-PSA-SPIONs on *P.aeruginasa* is only evident when they directly face SPION. This stressing effect could explain the increase in biofilm count. As seen in Fig. 6e, SZ-PSA-SPIONs did not inhibit pyoverdine production through 48 h treatment. Similarly, L3APimin did not inhibit the synthesis of pyoverdine for 48 h incubation period, while G-PDA strongly downregulated pyoverdine synthesis. The effect of SPION on pyoverdine synthesis was shown to be time dependent, they induce pyoverdine synthesis for the first 14 h while later on the rate of pyoverdine synthesis decreased [46].

Combination of SZ-PSA-, L3Apimin- and G-PDA-SPIONs with 10 μL of streptomycin/penicillin resulted in a decrease in the biofilm formation by 98 %, 95 % and 100 % in the case of 10^6 cfu/25 μL inoculum utilization (Supplementary Figure S9), where decrease in growth were respectively obtained as 85 %, 0% and 92 %. Based on the data, SZ-PSA and G-PDA provided strong synergistic effect with the antibiotic mixture. It is noteworthy to mention that only G-PDA strongly downregulated pyoverdine synthesis (Supplementary Figure S9) while it did not alter *P.aeruginosa* morphology grown on the coated fabric (Supplementary Figure S12). In the case of 10^4 cfu/25 μL inoculum utilization, combination with 20 μL and 10 μL of streptomycin/penicillin mixture resulted in the total elimination of growth and biofilm formation, where L3APimin, SZ-PSA and G-PDA individually decreased biofilm formation only by 32 %, 60 % and 42 % with 30–60 % decrease in growth, respectively (Supplementary Figure S8). It should be noted that the fluorescent pyoverdine synthesis was only strongly downregulated for MpAB-, SZ-PSA- and G-PDA-SPION treatments where L3Apimin- and bare SPION treatments did not show any effect for 24 h incubation period (Supplementary Figure S8), while pyoverdine synthesis was clear for all in 72 h incubation (Supplementary Figure S10). Increasing the incubation period up to 72 h resulted in growth of *P. auruginosa* for L3APimin SPIONs/streptomycin/penicillin treatment while combination of streptomycin/penicillin with either SZ-PSA- or G-PDA-SPIONs continued their antibacterial effect against *P. auruginosa* throughout 72 h incubation period (Supplementary Figure S10). L3APimin SPIONs coated fabric also did not alter morphology of *P.aeruginosa* (Supplementary Figure S11). It should be stated that the tested SPIONs did not fully preserve their colloidal character within the liquid media for 24 h; bare SPION, L3Apimin-SPION and SZ-PSA-SPION totally aggregated within 10 h incubation, while MpAB-SPION and G-PDA-SPION protected ~40 % colloidal character within 16 h incubation. Aggregation can be resulted from protein corona formation, and that did not show any correlation with the charge of the SPIONs, rather it was related to the surface chemistry. Aggregation reduces antibacterial capacity of the SPIONs. Another important observation was that aggregation behavior of the SPIONs showed dependence on the bacteria in the medium, which can be related to the differences in pH and released entities upon bacterial metabolism. For example, except L3APimin SPION, all the tested SPIONs preserved their colloidal character for 48 h only in the case of *P. aeruginosa*.

Pyoverdines are Fe^{3+} ion capturing proteins containing fluorescent groups, which are released into bacterial microenvironment for sustaining required metal ion uptake into the bacterial species, particularly for *Pseudomonas spp.* [47]. Pyoverdines play a key role in pathogenicity of *P.aeruginosa* by chelating iron ions from host proteins and triggering synthesis of virulence factors [48]. When behavior of *P. aeruginosa* was studied against $AgNO_3$ (100 μg/mL), $CuSO_4$ (100 μg/mL) and $FeCl_3$ (100

μg/mL) in comparison to control for 24 h treatment (Fig. 8). Ag^{+} ion gave very strong toxicity, where Cu^{2+} only decreased green color formation. Fe^{3+} did only downregulate the growth and pyoverdine synthesis for 24 h treatment. Increasing incubation period up to 48 h showed that Fe^{3+} and Cu^{2+} did not prevent aggressive growth. Introduction of MpAB-SPIONs on one side of the soft agar (Fig. 8b) even prevented pyoverdine synthesis of *P.aeruginosa*, which could be related to that even minute amount of MpAB-SPIONs release into *P.aeruginosa* growth environment can affect its pyoverdine synthesis under the tested conditions.

Synthesis of pyoverdine is strongly affected by the free metal ions and metallic nanostructures. When it comes to SPIONs, NP-bacterial membrane interaction and surface chemistry of the NP can interfere with the pyoverdine regulation metabolism [49], so it can be speculated that the difference between the tested free metal ions and the SPIONS can be related to the way they interfered the pyoverdine regulation of *P. aeruginosa*. In our studies, anti *P. aeruginosa* effect of the SPIONs showed dependence on the SPION/inoculum ratio and the SPION type, where different SL-SPIONs follow different trend. Organic matter content on the tested SPIONs were between 0.11 mg/mg to 0.47 mg/mg, whose effect was not observed neither for pyoverdine synthesis nor for biofilm formation along with growth. However, synergistic effect was clear between some of the SPIONs (based on the surface chemistry) and streptomycin/penicillin for all aspects in the case of *P. aeruginosa* inoculum utilization.

Since the SPIONs gave SL dependent synergistic enhancement to known antibiotics and altered bacterial metabolism, screening a variety of SLs decorated SPIONs towards a dedicated multi-drug resistant bacterial strain can bring out highly affective SL-SPIONs. Besides, in further studies, decoration of SPIONs with different amounts of a dedicated SLs can tune antibacterial capabilities of the SL-SPIONs, because of the fact that load of SLs on NPs can alter their orientation, which in turn alters their affinity to the lectins. Coating face masks with antimicrobial nanomaterials is currently a hot topic, and our preliminary studies reveal that the SPIONs can be useful for enhancing face masks for blocking and eliminating microorganisms.

4. Conclusions

The action of microwave-assisted hydrothermal method permitted to promote the recrystallization and, subsequently, functionalization of the SPIONs' surface directly with the SL, thus representing a key-step for the antibacterial action of a library of SL functionalized SPIONs. All the SPION samples present the corresponding SL traces on their surface, confirmed by FT-IR and ζ-potential analyses. Nanoparticles were observed to have average size in the range 4−6 nm, are single crystalline. Four SL-SPION samples, derived from different base sugars, with the highest negative surface charge in colloidal state have been chosen for further analysis, where their magnetization behavior was confirmed to be superparamagnetic. Furthermore, the fit of the magnetization curves, obtained through VSM analysis, allowed the estimation of magnetic core size, which directly affects the saturation magnetization of the functionalized SPIONs. Magnetic core size estimated is in the same order as the size estimated from the TEM micrographs. All the characterized samples would be then suitable for antibacterial action in solution, enabling the possibility of magnetic separation. Given the magnetic characterization, the microwave-assisted synthesis process did not alter the superparamagnetic characteristics of the samples, thus constituting a general methodology for functionalization of SPIONs surface with the synthesized carbohydrates with pre-defined functional entities. The usage of customized and on-purpose designed SL permitted to actively target specific sites of bacteria. The antibacterial tests showed, indeed, a great antibacterial activity depending on the sugar ligand chemistry, and the SPIONs elevated antibacterial activity of streptomycin/penicillin antibiotic mixture. Detailed studies performed on *P. aeruginosa* revealed that the SPIONS selectively downregulated pyoverdine synthesis and altered morphology of *P. aeruginosa* grown on coated fabrics. Finally, the use of extensive NP characterization tools together with antibacterial activity tests constituted an effective path towards the design and development of efficient structures against antibiotic-resistant bacterial species.

Declaration of Competing Interest

The authors declare that they have no known competing financial interests or personal relationships that could have appeared to influence the work reported in this paper.

Acknowledgements

This research was funded by the Wallenberg Foundation, and through the COST Action CA18132 - (GLYCOnanoPROBES) short term scientific mission (STSM). Prof. V. Korenivski and Dr. Mykola Kulyk are acknowledged for providing VSM characterization for magnetization studies of the SPIONs in this work. MST acknowledges the financial support from Olle Engkvist Foundation (SOEB) [190-0315] for the establishment of MW synthesis facilities.

Appendix A. Supplementary data

Supplementary material related to this article can be found, in the online version, at doi:https://doi.org/10.1016/j.colsurfa.2020.126086.

References

[1] I.D. Vukoje, E.S. Džunuzović, S. Dimitrijević, S. Phillip Ahrenkiel, J.M. Nedeljković, Size-dependent antibacterial properties of Ag nanoparticles supported by amino-functionalized poly(GMA-co-EGDMA) polymer, Polym. Compos. 40 (July 7) (2019) 2901–2907, https://doi.org/10.1002/pc.25120.

[2] A.O. Baskakov, et al., Magnetic and interface properties of the core-shell Fe 3 O 4 /Au nanocomposites, Appl. Surf. Sci. 422 (2017) 638–644, doi: 10.1016/j.apsusc.2017.06.029.

[3] N. Zhang, X. Yu, J. Hu, Synthesis of copper nanoparticle-coated poly(styrene-co-sulfonic acid) hybrid materials and its antibacterial properties, Mater. Lett. 125 (June) (2014) 120–123, https://doi.org/10.1016/j.matlet.2014.03.161.

[4] D.J. McClements, H. Xiao, Is nano safe in foods? Establishing the factors impacting the gastrointestinal fate and toxicity of organic and inorganic food-grade nanoparticles, NPJ Sci. Food 1 (December 1) (2017) 6, https://doi.org/10.1038/s41538-017-0005-1.

[5] J.S. Beveridge, J.R. Stephens, M.E. Williams, The use of magnetic nanoparticles in analytical chemistry, Annu. Rev. Anal. Chem. 4 (July 1) (2011) 251–273, https://doi.org/10.1146/annurev-anchem-061010-114041.

[6] T.Ahuja Rajesh, D. Kumar, Recent progress in the development of nano-structured conducting polymers/nanocomposites for sensor applications, Sens. Actuators B Chem. 136 (1) (2009) 275–286, https://doi.org/10.1016/j.snb.2008.09.014.

[7] M.A. Busquets, J. Estelrich, M.J. Sánchez-Martín, Nanoparticles in magnetic resonance imaging: from simple to dual contrast agents, Int. J. Nanomed. 10 (March 1) (2015) 1727, https://doi.org/10.2147/IJN.S76501.

[8] L. Storozhuk, N. Iukhymenko, Iron oxide nanoparticles modified with silanes for hyperthermia applications, Appl. Nanosci. 9 (July 5) (2019) 889–898, https://doi.org/10.1007/s13204-018-0777-x.

[9] E. Mettler, et al., Magnetic separation of encapsulated islet cells labeled with superparamagnetic iron oxide nano particles, Xenotransplantation 20 (July 4) (2013) 219–226, https://doi.org/10.1111/xen.12042.

[10] D. Lachowicz, et al., A hybrid system for magnetic hyperthermia and drug delivery: SPION functionalized by curcumin conjugate, Materials (Basel) 11 (November 12) (2018) 2388, doi: 10.3390/ma11122388.

[11] C. Justin, S.A. Philip, A.V. Samrot, Method of synthesis of SPIONs, Appl. Nanosci. 7 (7) (2017) 463–475, https://doi.org/10.1007/s13204-017-0583-x.

[12] M.B. Gawande, S.N. Shelke, R. Zboril, R.S. Varma, Microwave-assisted chemistry: synthetic applications for rapid assembly of nanomaterials and organics, Acc. Chem. Res. 47 (April 4) (2014) 1338–1348, https://doi.org/10.1021/ar400309b.

[13] N. Saxena, N. Dholia, S. Akkireddy, A. Singh, U.C.S. Yadav, C.L. Dube, Efficient microwave synthesis, functionalisation and biocompatibility studies of SPION based potential nano-drug carriers, Appl. Nanosci. (2019), https://doi.org/10.1007/s13204-019-01153-8.

[14] E. Carenza, V. Barceló, A. Morancho, J. Montaner, A. Rosell, A. Roig, Rapid synthesis of water-dispersible superparamagnetic iron oxide nanoparticles by a microwave-assisted route for safe labeling of endothelial progenitor cells, Acta Biomater. 10 (August 8) (2014) 3775–3785, https://doi.org/10.1016/J.ACTBIO.2014.04.010.

[15] C. Janko, et al., Functionalized superparamagnetic iron oxide nanoparticles (SPIONs) as platform for the targeted multimodal tumor therapy, Front. Oncol. 9 (February) (2019). Frontiers Media S.A.doi: 10.3389/fonc.2019.00059.
[16] M.S. Toprak, B.J. McKenna, M. Mikhaylova, J.H. Waite, G.D. Stucky, Spontaneous assembly of magnetic microspheres, Adv. Mater. 19 (May 10) (2007) 1362–1368, https://doi.org/10.1002/adma.200602114.
[17] G.M. Saladino, B. Hamawandi, C. Vogt, G.K. Rajarao, M.S. Toprak, Click chemical assembly and validation of bio-functionalized superparamagnetic hybrid microspheres, Appl. Nanosci. (2020), https://doi.org/10.1007/s13204-020-01274-5.
[18] B.S. Kim, D.J. Hong, J. Bae, M. Lee, Controlled self-assembly of carbohydrate conjugate rod-coil amphiphiles for supramolecular multivalent ligands, J. Am. Chem. Soc. 127 (46) (2005) 16333–16337, https://doi.org/10.1021/ja055999a.
[19] Á.G. Barrientos, J.M. De la Fuente, T.C. Rojas, A. Fernández, S. Penadés, Gold glyconanoparticles: synthetic polyvalent ligands mimicking glycocalyx-like surfaces as tools for glycobiological studies, Chem. Eur. J. 9 (9) (2003) 1909–1921, https://doi.org/10.1002/chem.200204544.
[20] K.K. Katti, V. Kattumuri, S. Bhaskaran, K.V. Katti, R. Kannan, Facile and general method for synthesis of sugar-coated gold nanoparticles, Int. J. Green Nanotechnol. Biomed. 1 (1) (2009) 1–8, https://doi.org/10.1080/19430850902983848.
[21] T.C. Rojas, J.M. De La Fuente, A.G. Barrientos, S. Penadés, L. Ponsonnet, A. Fernández, Gold glyconanoparticles as building blocks for nanomaterials design, Adv. Mater. 14 (8) (2002) 585–588, doi: 10.1002/1521-4095(20020418)14:8<585::AID-ADMA585>3.0.CO;2-W.
[22] A.J. Reynolds, A.H. Haines, D.A. Russell, Gold glyconanoparticles for mimics and measurement of metal Ion-mediated carbohydrate - carbohydrate interactions, Langmuir 22 (3) (2006) 1156–1163, https://doi.org/10.1021/la052261y.
[23] S. Fernando, T. Gunasekara, J. Holton, Antimicrobial Nanoparticles: applications and mechanisms of action, Sri Lankan J. Infect. Dis. 8 (May 1) (2018) 2, https://doi.org/10.4038/sljid.v8i1.8167.
[24] X. Yang, L. Zhang, X. Jiang, Aminosaccharide – gold nanoparticle assemblies as narrow-spectrum antibiotics against methicillin-resistant Staphylococcus aureus, Nano Res. 11 (12) (2018) 6237–6243.
[25] M.M. Tajkarimi, S.A. Ibrahim, D.O. Cliver, Antimicrobial herb and spice compounds in food, Food Control (2010), https://doi.org/10.1016/j.foodcont.2010.02.003.
[26] M.K. Paczosa, J. Mecsas, Klebsiella pneumoniae : going on the Offense with a Strong Defense, Microbiol. Mol. Biol. Rev. 80 (3) (2016) 629–661, https://doi.org/10.1128/MMBR.00078-15.Address.
[27] Y. Li, P. Leung, L. Yao, Q.W. Song, E. Newton, Antimicrobial effect of surgical masks coated with nanoparticles, J. Hosp. Infect. 62 (1) (2006) 58–63, https://doi.org/10.1016/j.jhin.2005.04.015.
[28] H.S. Jeong, et al., Facile and rapid direct gold surface immobilization with controlled orientation for carbohydrates, Bioconjug. Chem. 18 (2007) 2197–2201, doi: 10.1021/bc700288z.
[29] İ. Yazgan, Synthesis of open-chain sugar derivatives As anticancer and antimicrobial agents, Commun. Fac. Sci. Univ. Ankara Ser. C Biol. 28 (2) (2019) 148–159.
[30] Y. Ahn, E.J. Choi, S. Kim, H.N. Ok, Magnetization and Mössbauer study of cobalt ferrite particles from nanophase cobalt iron carbonate, Mater. Lett. 50 (August 1) (2001) 47–52, https://doi.org/10.1016/S0167-577X(00)00412-2.
[31] J. Coates, Encyclopedia of analytical chemistry -IInterpretation of infrared spectra, a practical approach, Encycl. Anal. Chem. (2004) 1–23.
[32] G.M. Saladino, SPfit - Superparamagnetic Fit, Zenodo, June, 2019, https://doi.org/10.5281/ZENODO.3244439.
[33] R. Chantrell, J. Popplewell, S. Charles, Measurements of particle size distribution parameters in ferrofluids, IEEE Trans. Magn. 14 (September 5) (1978) 975–977, https://doi.org/10.1109/TMAG.1978.1059918.
[34] E.P. Ivanova, et al., Differential attraction and repulsion of Staphylococcus aureus and Pseudomonas aeruginosa on molecularly smooth titanium films, Sci. Rep. 165 (1) (2011) 1–8, doi: 10.1038/srep00165.
[35] W. Bing, H. Sun, Z. Yan, J. Ren, X. Qu, Programmed Bacteria death induced by carbon dots with different surface charge, Small (34) (2016) 4713–4718, https://doi.org/10.1002/smll.201600294.
[36] I. Yazgan, N. Du, R. Congdon, V. Okello, O.A. Sadik, Biofunctionalized poly (amic) acid membranes for absolute disinfection of drinking water, J. Memb. Sci. 472 (2014) 261–271, https://doi.org/10.1016/j.memsci.2014.07.048.
[37] I. Yazgan, N.M. Noah, O. Toure, S. Zhang, O.A. Sadik, Biosensor for selective detection of E. Coli in spinach using the strong affinity of derivatized mannose with fimbrial lectin, Biosens. Bioelectron. 61 (2014), https://doi.org/10.1016/j.bios.2014.05.008.
[38] I. Yazgan, et al., Selective sensing and imaging of Penicillium italicum spores and hyphae using carbohydrate-lectin interactions, ACS Sens. 3 (3) (2018) 648–654, doi: 10.1021/acssensors.7b00934.
[39] C. Wu, G. Rubasinghege, I.A. Mudunkotuwa, C. Caraballo, Iron oxide nanoparticles induce Pseudomonas and inhibit antimicrobial peptide function, Environ. Sci. Nano 1 (2014) 123–132, https://doi.org/10.1039/c3en00029j.
[40] Y. Liu, L. He, A. Mustapha, H. Li, Z.Q. Hu, M. Lin, Antibacterial activities of zinc oxide nanoparticles against Escherichia coli O157:H7, J. Appl. Microbiol. 107 (4) (2009) 1193–1201, https://doi.org/10.1111/j.1365-2672.2009.04303.x.
[41] V.T. Orlandi, F. Bolognese, L. Chiodaroli, T. Tolker-Nielsen, P. Barbieri, Pigments influence the tolerance of pseudomonas aeruginosa PAO1 to photodynamically induced oxidative stress, Microbiol. (United Kingdom) 161 (12) (2015) 2298–2309, https://doi.org/10.1099/mic.0.000193.
[42] D.R. Kirienko, D. Kang, N.V. Kirienko, Novel pyoverdine inhibitors mitigate Pseudomonas aeruginosa pathogenesis, Front. Microbiol. 10 (January) (2019) 1–14, https://doi.org/10.3389/fmicb.2018.03317.
[43] B. Ramalingam, T. Parandhaman, S.K. Das, Antibacterial Effects of Biosynthesized Silver Nanoparticles on Surface Ultrastructure and Nanomechanical Properties of Gram- Negative Bacteria viz. Escherichia coli and Pseudomonas aeruginosa, ACS Appl. Mater. Interfaces 8 (2016) 4963–4976, https://doi.org/10.1021/acsami.6b00161.
[44] J. Zhao, Z. Wang, Y. Dai, B. Xing, Mitigation of CuO nanoparticle-induced bacterial membrane damage by dissolved organic matter, Water Res. 47 (12) (2013) 4169–4178, https://doi.org/10.1016/j.watres.2012.11.058.
[45] M. Arakha, M. Saleem, B.C. Mallick, S. Jha, The effects of interfacial potential on antimicrobial propensity of ZnO nanoparticle, Sci. Rep. 5 (2015) 1–10, https://doi.org/10.1038/srep09578.
[46] D. Creanga, U. Alexandru, I. Cuza, A. Airinei, Fluorescence of pyoverdine synthesized by Pseudomonas under the effect of iron oxide nanoparticles Fluorescence of pyoverdine synthesized by Pseudomonas under the effect of iron oxide nanoparticles, Rom. Biotechnol. Lett. 16 (4) (2011) 6336–6343.
[47] I.J. Schalk, L. Guillon, Pyoverdine biosynthesis and secretion in Pseudomonas aeruginosa : implications for metal homeostasis, Environ. Microbiol. 15 (6) (2013) 1661–1673, https://doi.org/10.1111/1462-2920.12013.
[48] D. Kang, D.R. Kirienko, P. Webster, A.L. Fisher, Pyoverdine, a siderophore from Pseudomonas aeruginosa, translocates into C. Elegans, removes iron, and activates a distinct host response, Virulence 9 (1) (2018) 804–817.
[49] M. Magro, et al., Enlightening mineral iron sensing in Pseudomonas fluorescens by surface active maghemite nanoparticles : involvement of the OprF porin, BBA Gen. Subj. 1860 (10) (2016) 2202–2210, https://doi.org/10.1016/j.bbagen.2016.05.007.